Hindawi
Shock and Vibration
Volume 2022, Article ID 2924836, 19 pages
https://doi.org/10.1155/2022/2924836

Research Article

Seismic Performance Assessment of Ordinary Moment Resisting Frame Equipped with Viscous Dampers under Pulse-Like Earthquakes

Amir Yousefpour, Hamid Mazidababdi Farahani, and Mohsen Ali Shayanfar

Department of Civil Engineering, Iran University of Science and Technology, Tehran, Iran

Correspondence should be addressed to Amir Yousefpour; amir_yousefpour@cmps2.iust.ac.ir

Received 17 October 2021; Accepted 27 January 2022; Published 31 March 2022

Academic Editor: Jiaqiang E

In conventional structures, the earthquake-resistant design is based on flexibility after yielding of structural members to provide a loss of earthquake input energy, while, using dampers, the input energy loss can be concentrated in predetermined points to prevent the nonlinear behavior of the main members that are also in the gravity bearing path. However, near-fault earthquakes might cause unexpected failure and severe structural damage, especially those with the pulse-like effect. A pulsed movement in the near field records in this system will, however, result in unusual behavior. Technology advances and the creation of vibration control systems have helped control this type of behavior since the earthquake forces are applied indirectly to the structure. For further investigation of this issue, in this study, some traditional two-dimensional frames were modeled for 3, 8, and 12 floors. Seven near-fault pulsed and seven far-fault nonpulsed accelerometers are applied. The structural behavior in four modes is examined: (1) without damper and soil-structure interaction effect, (2) without damper and considering soil-structure interaction effect, (3) with damper and considering soil-structure interaction, and (4) with damper without considering soil-structure interaction. Each model is analyzed in OpenSees software under incremental dynamic analysis. Then, the fragility curve is plotted based on the results. The results indicate that frame (4) reaches the failure level at a higher spectral acceleration, which means that the performance of the viscous damper in reducing drift between floors is one of the main criteria for predicting damages. It also shows the effect of soil-structure interaction on increasing the drift between floors and reaching failure at lower spectral acceleration in all models. Also, by comparing the fragility curves of the models under near-field and far-field records, it is found that the probability of failure under far-field documents (without pulse) is less than that under near-field documents (with a pulse).

1. Introduction

During ground motions, much energy is applied to the structure. If this energy exceeds the capacity, it will cause damage to the member and eventually the entire network. On the other hand, long-period pulses in near-field earthquakes weaken the performance of systems. Many researchers like MacRae et al. [1], Tothong and Cornell [2], Alavi and Krawinkler [3], Hall et al. [4], Champion and Liel [5], and Özuygur and Noroozinejad [6] have examined the dynamic response of the structures in the near-fault region. The key conclusion regarding the effect of near-fault ground motions on structural response is that near-fault pulse-like records tend to increase the displacement response in structures relative to nonpulse-like movements. These displacement demands could increase structural and nonstructural damage. The pulse-like earthquake generally imposes a high seismic need on the structure, so the damper must resist the earthquake motion. Experiments have demonstrated that dampers can dissipate more than 90% of the total earthquake input energy [7].

For this purpose, an energy dissipation system transfers some of the energy applied to the structure to this device, thus minimizing the damage to the structure. In recent decades, energy dissipation systems in structures have been widely used to reduce the forces caused by earthquakes and

reduce the lateral displacement of buildings within the limits of the code. One type of these consumables, as passive control systems, is viscous dampers, which have attracted the attention of many researchers like Zahrai and Mohammadi [8] and Silwal et al. [9]. A viscous damper consists of a piston with some orifices inside the cylinder containing highly viscous fluid. Energy dissipation of this damper is through pushing viscous fluid out of the orifices. Luo et al. [10] examined the effects of stochastic traffic loads, corrosion, and fatigue on aging polymer composite bridges. In this study, numerical data were used to estimate the fatigue life of a PC bridge and to maintain it as it ages. According to Zhang et al. [11], the time-harmonic point-, ring-, and disc-loadings of the soil at the inner surface and the rigid foundation caused the soil layer to exhibit three-dimensional intensity Green's functions. Liu et al. [12] examined 3-dimensional ground-penetrating radar imaging to detect road cavities in urban areas. Morai-dastjerdi et al. [13] investigated the mesh-free dynamic analysis of FGM sandwich plates resting on an elastic base. Accordingly, Ghaffarzadeh et al. [14] analyzed the seismic response of building frames supplemented with variable orifice dampers under near-fault earthquakes. They found out that the influence of the pulse effect on seismic performance of damper systems has not been well understood because of the individual differences in each near-fault earthquake record. Prasad and Mazumder [15] investigated the seismic response of a set of steel buildings with and without viscous dampers installed in the inner bay for energy dissipation. Viscous dampers were reported to reduce the displacements, which decreased the amount of steel needed for the overall stability. Wang et al. [16] used a gas physisorption test (CO_2 and N_2) to analyze pore heterogeneity and its underlying causes in overmature Wufeng-Longmaxi shales and their isolated organic matter (OM). Jiang et al. [17] studied tectonothermal histories of the Dongpu Depression from thirteen wells to reconstruct Cenozoic tectonothermal histories. Zhang et al. [18] investigated the progress of friction-based seismic isolation and energy dissipation technologies.

The study conducted by Balkanlou et al. [19] demonstrated that the structure with dampers could be designed optimally to justify the cost spent using dampers. Silvestri et al. [20] proposed a five-step procedure for creating viscous dampers to achieve target performance levels. Using viscous dampers to mitigate the pounding of the adjacent buildings was the subject of Milanchian and Hosseini's research [21]. Nonlinear and linear viscous dampers interconnected the buildings to provide vertical seismic isolation. The final results did not indicate a preferable performance of nonlinear viscous dampers over linear viscous dampers. However, the authors revealed that employing appropriate link parameters proportional to mass and stiffness ratios could lead to satisfactory levels of seismic response reduction in cases of both types of dampers. De Demonico et al. [22] gave energy-based perspectives to interpret the seismic performance in terms of the dissipated energy by the viscous dampers out of the total earthquake-induced energy. Xu et al. [23] constructed a model for the coupling of water, heat, and solute transport in saline loess, taking sodium sulfate crystallization into account. Li et al. [24] investigated the feasibility and drawbacks of applying the PFDD technique to combat FDI assaults on power grid state estimates. Wang et al. [25] suggested a novel technique for bioinspired defect diagnostics based on rough sets (RSBFDM). The suggested solution outperforms existing options in experiments conducted on genuine 110 kV and 750 kV substations.

Moreover, in conventional structural analysis and design, the effect of soil beneath the foundation is mainly ignored. However, Ghalami [26] indicates that soil flexibility may have a significant impact on the structural response. Amiri et al. [27] evaluated several three-dimensional steel moment-resisting frames to investigate the effect of soil-structure interaction (SSI) in structural retrofitting. The studied models were considered three-dimensional models of 3-, 7-, and 13-story steel moment-resisting frames. The analysis results showed that considering the soil-structure interaction increases the natural period of the structure. The results also show that the number of buildings' natural period increases in soil-structure interaction. However, this effect can be ignored in low-rise structures. Šago et al. [28] have identified many of the several obstacles that occurred concurrently with the COVID-19 epidemic and the severe earthquake in Zagreb. The findings indicate that quick developments broadened our area of practice without delay during these exceedingly trying times. Xu et al. [29] used the reactive Euler equations coupled with a comprehensive chemical model to study the interactions between two ODWs created by symmetrical finite wedges in hydrogen-air mixtures. Arbabi and Tahghghi [30] simulated multistory building-foundation systems through a Winkler-based approach using OpenSees finite element framework. Four typical 4-, 8-, 12-, and 16-story steel moment-resisting frame (MRF) buildings on three hypothetically soft, medium, and hard soil sites with shear wave velocities less than 600 m/s subjected to actual ground motion records of varied hazard levels are modeled with and without SSI. It is observed that the performance level of models supported by the flexible foundation, particularly in an intense earthquake event, may alter significantly in comparison to fixed-base structures. Moreover, for MRFs on soft soil, the nonlinear foundation is found to have a significant effect on the force and displacement demands. The authors indicate the necessity of considering the SSI effect to accomplish an economical yet safe structural design.

In this study, an ordinary two-dimensional moment-resisting steel frame of 3, 8, and 12 floors was designed under seven near-fault pulsed records and seven far-fault non-pulsed records. Despite the fact that ordinary moment resisting frames are widely used, they do not comply with special detailing requirements for ductile behavior. It is, therefore, essential to evaluate the behavior of these frames in the presence of dampers and SSI effects. The structural behavior was examined in four modes: (1) without damper and soil-structure interaction (SSI) effect; (2) without damper and considering SSI effect; (3) with damper and considering SSI; and (4) with damper without considering SSI. OpenSees software analyzed each model under incremental dynamic analysis (IDA). Then, based on the results of a comprehensive active study, the fragility curve was drawn. Vulnerability levels introduced in HAZUS MH-MR4 [31]

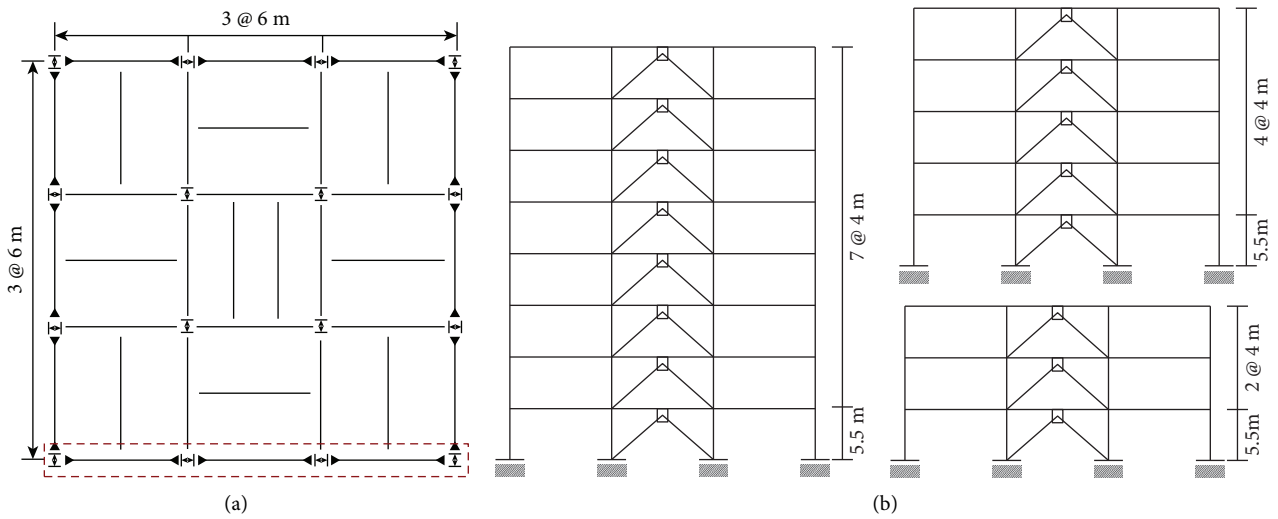

Figure 1: An analysis of model structures: (a) structural plans; (b) elevations of structures that include dampers [34].

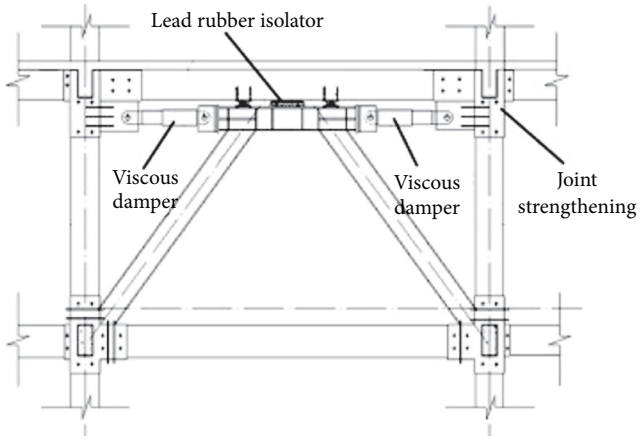

Figure 2: Configuration of viscous dampers [35].

Table 1: Basic information of studied buildings.

No. Stories	Fundamental period	Added damping ratio	Reflection coefficient	Seismic coefficient
3-Story	0.5454	0.1	2.75	0.165
8-Story	1.1381	0.1	1.848	0.1109
12-Story	1.5425	0.1	1.471	0.0883

were used to investigate different failure modes in the models. Finally, the performance of the building-damper system under near-fault pulsed-like earthquakes and the SSI effect are systematically investigated.

2. Details of Steel Frames, Modeling, and Analysis

In this research, three ordinary moments resisting steel frames of 3, 8, and 12 stories are modeled by the LRFD method [32]. Each frame has three openings with 5 meters and a floor height of 3.2 meters. The dead load in the structure's design was 500 kg/m, and the live load was 200 kg/m [33]. HEB profile was used for column design, and IPE profile was used for beam. Double channel is used for bracing elements (see Figure 1).

Also, for Incremental Dynamic Analysis (IDA), by assigning values of 0.1 g to 3 g for each acceleration, the analyses were performed for four modes of the frame, frame with damper, frame with soil-structure interaction, and frame with damper and soil-structure interaction.

Dampers were considered as diagonal members, as part of a chevron brace, horizontally at the top. The horizontal chevron configuration is applied here, as shown in Figure 2.

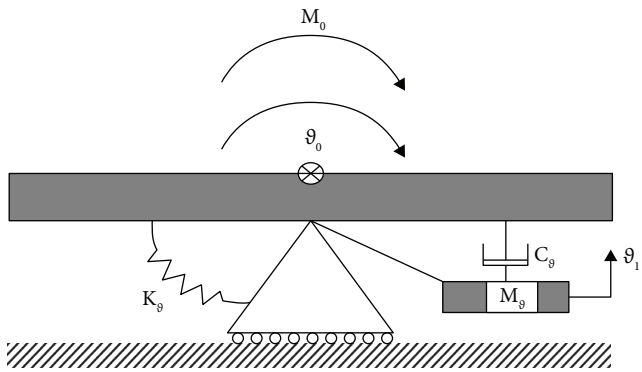

Figure 3: Spring-dashpot-mass model with an additional internal degree of freedom for the rotational degree of freedom [37].

Table 2: Detailed parameters for the springs used to consider the SSI effect.

	Spring stiffness	γ_0	μ_0
Vertical	$4G.r_0/1-u$	0.58	0.095
Horizontal	$8G.r_0/1-u$	0.85	0.27
Rocking	$8G.r_0^3/3\,(1-u)$	$1+\frac{0.3/3\,(1-\nu)m}{8r_o 5p}$	0.24

This system was proposed by Lu and Zhou and tested on a shaking table in 2002 [35]. Two viscous dampers are installed in a parallel way and supported by a steel chevron brace. Lead rubber bearings are installed at the top of the brace to keep the brace's stability and dissipate the energy under minor earthquakes.

The added damping ratio, reflection coefficient, seismic coefficient, and entire period of the studied buildings are summarized in Table 1. It is necessary to explain that the additional damping ratio is an important indicator for evaluating the damping effect of structures with energy-dissipation devices [36].

For modeling in OpenSees software, viscous material was used to design the damper. The Winkler model (BNWF) was modeled on the soil and foundation system linearly and nonlinearly. The infinite underlying soil medium is modeled using the concept of Cone Models with vertical, horizontal, and rocking degrees of freedom, as shown in Figure 3 and Table 2. A spring and a damper are introduced for each degree of freedom, which shows the effect of soil on that degree of freedom.

Selecting the appropriate seismic and failure intensity parameters to use IDA analysis is important and influential. Also, the selection of a proper seismic intensity parameter, in addition to causing less scattering and thus greater generality of the response created in the structure under the effect of earthquake records, must include the dynamic characteristics of a document such as frequency content and energy (Vamvatsikos and Cornell, 2002) [38]. To enter the main rotation time of the structure into the field of scaling records and consider the parameters of vibration and damping time, the spectral acceleration of the first model of the structure Sa (T_1) has been used as a measure of seismic intensity.

In this study, failure modes defined in the HAZUS MH-MR4 guidelines were used (National Institute of Building Sciences, 2004). Failure modes were introduced in the HAZUS instruction for steel buildings with a moment frame system with low and medium. In high stories, four failure modes are considered based on the Interstory DRIFT ratio: slight mode and moderate, extensive failure mode, and complete failure mode. Numerical values for each failure mode are presented in the Table 3 (see Table 3).

The DRIFT value obtained for each model under each of the earthquake records is compared with the values presented in the table above to check the arrival or passage of each model in each PGA value to each of these failure states.

(i) Fragility curve: to draw the fragility curve, a fragility function is required. The fragility function is a conditional probability, which expresses the possibility of failure of a structure at a certain level of failure or beyond for a given earthquake intensity. When the seismic requirements and structural capacity follow the normal log probability distribution, the fragility equation according to the HAZUS instruction is given as follows:

Table 3: Interstory Drift ratio in 4 failure modes according to HAZUS.

Type	Slight	Moderate	Extensive	Complete
S1L	0.006	0.012	0.03	0.08
S1M	0.004	0.008	0.02	0.0533
S1H	0.003	0.006	0.015	0.04

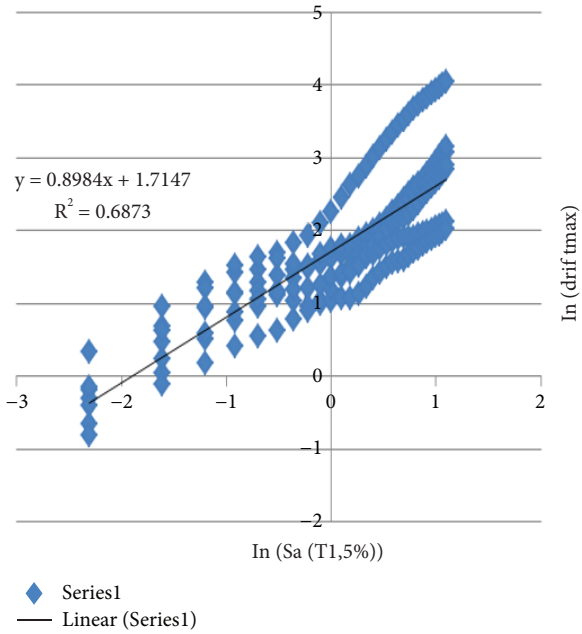

Figure 4: Maximum probabilistic seismic requirement for the relative displacement of floors.

Table 4: Different types of Steel moment frames in HAZUS MH-MR4 instruction.

Models name	Type of structural system		Number of stories
S1L	Steel moment frame	Low-rise	1–3
S1M		Mid-rise	4–7
S1H		High-rise	+8

$$P[C - D \leq 0.0|IM] = \varphi\left[\frac{\ln\left(S_d/S_c\right)}{\sqrt{\beta_{DI\ M}^2 + \beta_C^2}}\right]. \quad (1)$$

Respectively, the standard logarithm deviations are in capacity and need. The mean value of the limit state or seismic capacity and the mean value of the seismic requirement are the Intensity Measure (IM) function and the normal cumulative distribution function. The discount is combined according to the HAZUS instructions and converted to a parameter. Finally, the fragility relationship is written as follows:

Table 5: Values provided for S_c and β_{sd} for Steel moment frames in HAZUS MH-MR4 instruction.

Type	S_c	$_{sd}\beta$	S_c	$_{sd}\beta$	S_c	$_{sd}\beta$	S_c	$_{sd}\beta$
S1L	1.3	0.80	2.59	0.76	6.48	0.69	17.28	0.72
S1M	2.16	0.65	4.32	0.66	10.80	0.67	28.80	0.74
S1H	3.37	0.64	6.74	0.64	16.85	0.65	44.93	0.67

Table 6: Near-field earthquakes characteristics.

Record no.	Earthquake name	Station	Occurrence time	Magnitude	Epicentral distance (km)
1	Chi-chi, Taiwan	TCU120	1999	7.62	9.96
2	Darfield, New Zealand	Lincoln School	2010	7	5.28
3	Imperial Valley-06	El Centro Array #4	1979	6.53	4.9
4	Kobe, Japan	CEOR Station	1995	6.9	3.31
5	Morgan Hill	Gilroy Array #6	1984	6.19	3.45
6	Northridge-01	Pacoima Dam	1994	6.69	3.16
7	Parkfield-02, CA	CSMIP station 36419	2004	6	4.81

Table 7: Far-field earthquakes characteristics.

Record no.	Earthquake name	Station	Occurrence time	Magnitude	Epicentral distance (km)
8	Cape Mendocino	CSMIP station 89156	1992	7.01	16.54
9	Friuli, Italy-01	Bolzano	1976	6.5	33.32
10	Imperial Valley-06	Niland Fire Station	1979	6.53	35.2
11	Landers	Yermo Fire Station	1992	7.28	26.96
12	Northridge-01	LA - Saturn st	1994	6.69	27.0
13	San Fernando	OWNER station 0220	1971	6.61	22.77
14	Tabas, Iran	Dayhook	1978	7.35	24.07

$$Pf = \varphi\left[\frac{\ln\left(S_d/S_c\right)}{\beta_{s\,d}}\right]. \quad (2)$$

The parameter S_d is the average value of the seismic requirement obtained from the following equation:

$$\ln\left(S_d\right) = a.\ \ln\left(IM\right) + b. \quad (3)$$

In this equation, IM is the measure of seismic intensity, considered $\mathrm{Sa}(T_1)$ in this paper. a and b are regression coefficients obtained through linear regression analysis with the number of damage situations against different Sa. The X-Axis is the spectral acceleration parameter corresponding to the structure's first mode for each step. Its Y-axis is the logarithm of the criterion of maximum damage intensity and the relative displacement of the floors in each step. Figure 4 shows an example of the relationship between Sa (T_1) and the Engineering Demand Parameter (EDP), which is the maximum relative displacement of the floors in a logarithmic environment.

The values in the HAZUS MH-MR4 instruction are given for different types of constructions and other failure modes, which are shown in the following table (Tables 4–7).

3. Earthquake Excitations

The earthquake record selection should be made so that the analysis results include all the behavioral states of the structure in the range of elastic, plastic, and complete failure [39] although the soil type should be the same for the selected records so that the documents have a good resemblance to each other. The higher the number of forms used, the more valid the analysis results. On the other hand, adding the number of records will increase the analysis time and output volume. Therefore, seven near-field accelerometers and seven far-field accelerometers with the following characteristics have been used in this research [40].

The selected earthquakes have the following specifications:

(i) Occur in soil type 3.

(ii) Magnitude between 6 and 9 Richter.

(iii) Epicentral distance for near-field earthquakes is below 10 km, and for far-field earthquakes, it is above 15 km.

(iv) To maintain the seismic parameter of near-fault ground motions, they are not scaled [41].

4. Results

In the following, the analysis results of two-dimensional 3-, 8-, and 12-story steel moment frames in the form of IDA curves in 16%, 50%, and 84% percentiles and fragility curves are presented.

4.1. Three-Story Frame. The summary of the IDA curve with 16%, 50%, and 84% percentiles and fragility curves in a 3-

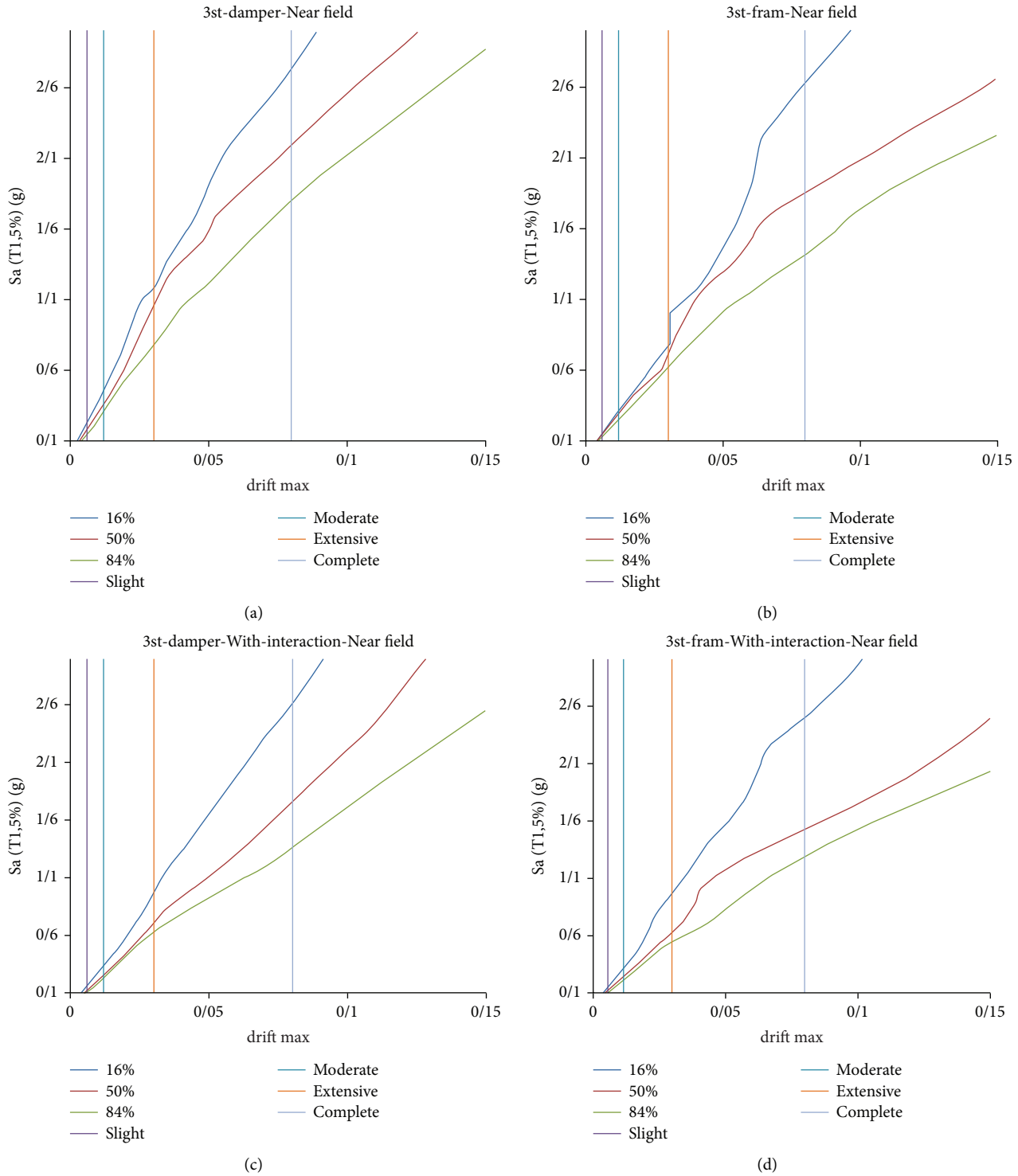

Figure 5: Summary of IDA curves for 16%, 50%, and 84% percentiles in 3-story Ordinary moment resisting frame affected by near-field earthquakes. Examined cases: (a) with damper without considering SSI; (b) without Damper and SSI effect; (c) with damper and considering SSI; (d) without damper but considering SSI effect.

story frame under seven pairs of near-field and far-field earthquakes is presented.

As can be seen, the slope of the linear region in the (a) case, with damper and without considering SSI, is less than that in other cases, which shows a softer behavior. In the case of the damper, it enters the collapse region at a higher acceleration, which indicates better performance than other cases. Considering that the criterion of damage is interstory drift, the results of the above diagram show that the frame with damper reaches the level of failure at a higher spectral

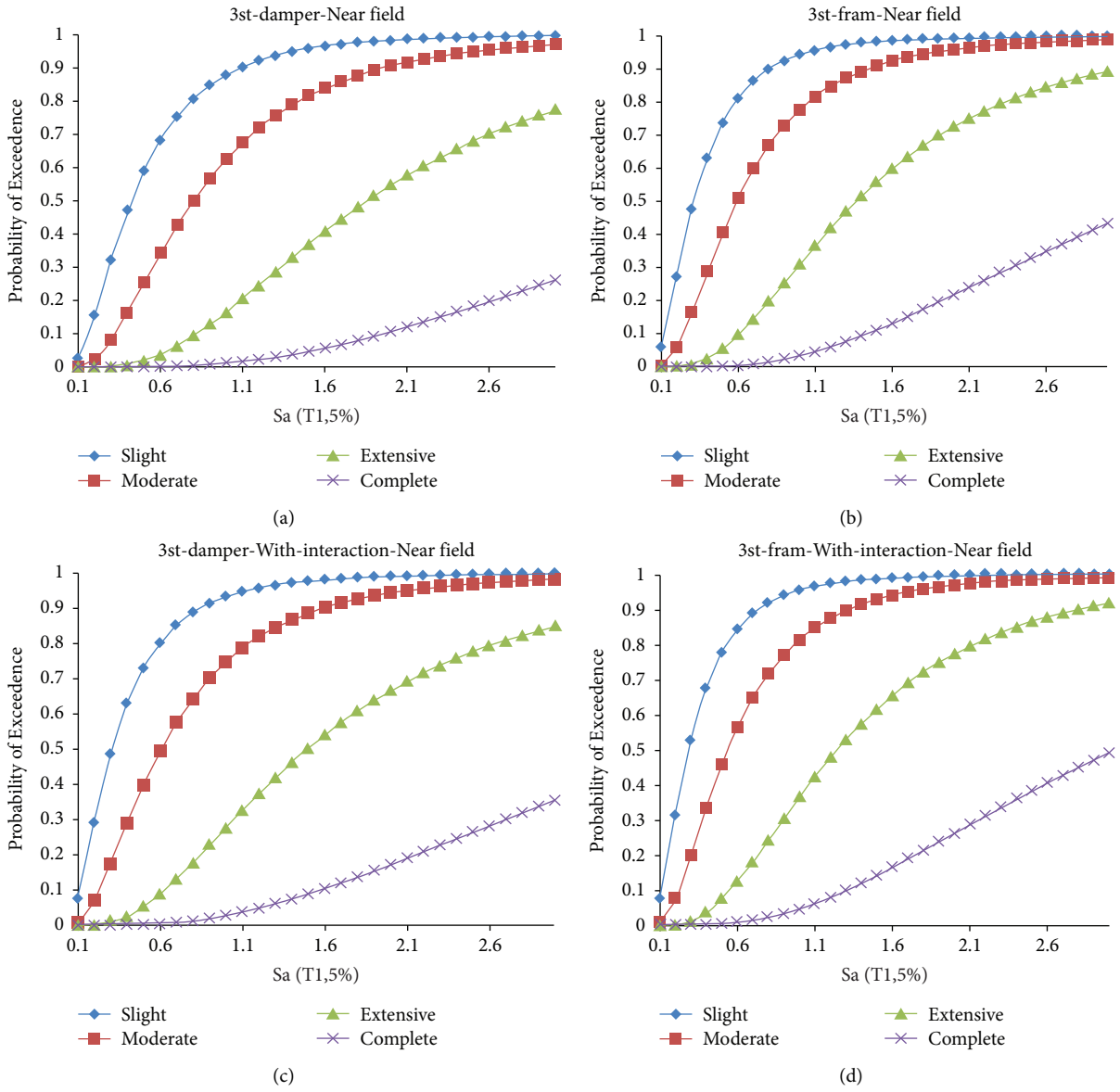

Figure 6: Fragility curves in 3-story ordinary moment resisting frame affected by near-field earthquakes. Examined cases: (a) with damper without considering SSI; (b) without Damper and SSI effect; (c) with damper and considering SSI; (d) without damper but considering SSI effect.

acceleration, respectively, compared to the frame without soil-structure interaction, the frame with soil-structure interaction, and the damper and the frame with interaction. This indicates the damper's performance in reducing interstory drift as one of the criteria for predicting damage and shows the effect of soil-structure interaction on increasing displacement between floors and reaching the level of failure at lower spectral acceleration. The fragility curves of 3-story frames under seven pairs of near-field acceleration are shown in Figures 5 and 6.

The fragility curve shows that the probability of structural failure in low failure mode occurs in less Sa values, and moderate, extensive, and complete failure modes occur in higher Sa values. In all curves, for low and moderate failure situations, the slope of the curve is first increased and then decreased. For extensive failure mode, the angles change with an almost uniform slope. For complete failure mode, the slope changes are extremely small. According to the coefficient of acceleration scale of near field earthquakes for 3-story structures, fragility occurs at a spectral acceleration of 1.284 g for type three soil. The results also show that soil-structure interaction has a significant effect on increasing the probability of structural failure. Also, dampers in both cases with and without soil-structure interaction reduce the likelihood of failure. In the following, a summary of the IDA curve of a 3-story frame under seven pairs of far-field earthquakes is shown in Figure 7.

The slope of the linear region in case (a), with damper and without SSI, is less than that in other states, which shows a softer behavior. In the cases with the damper, it enters the

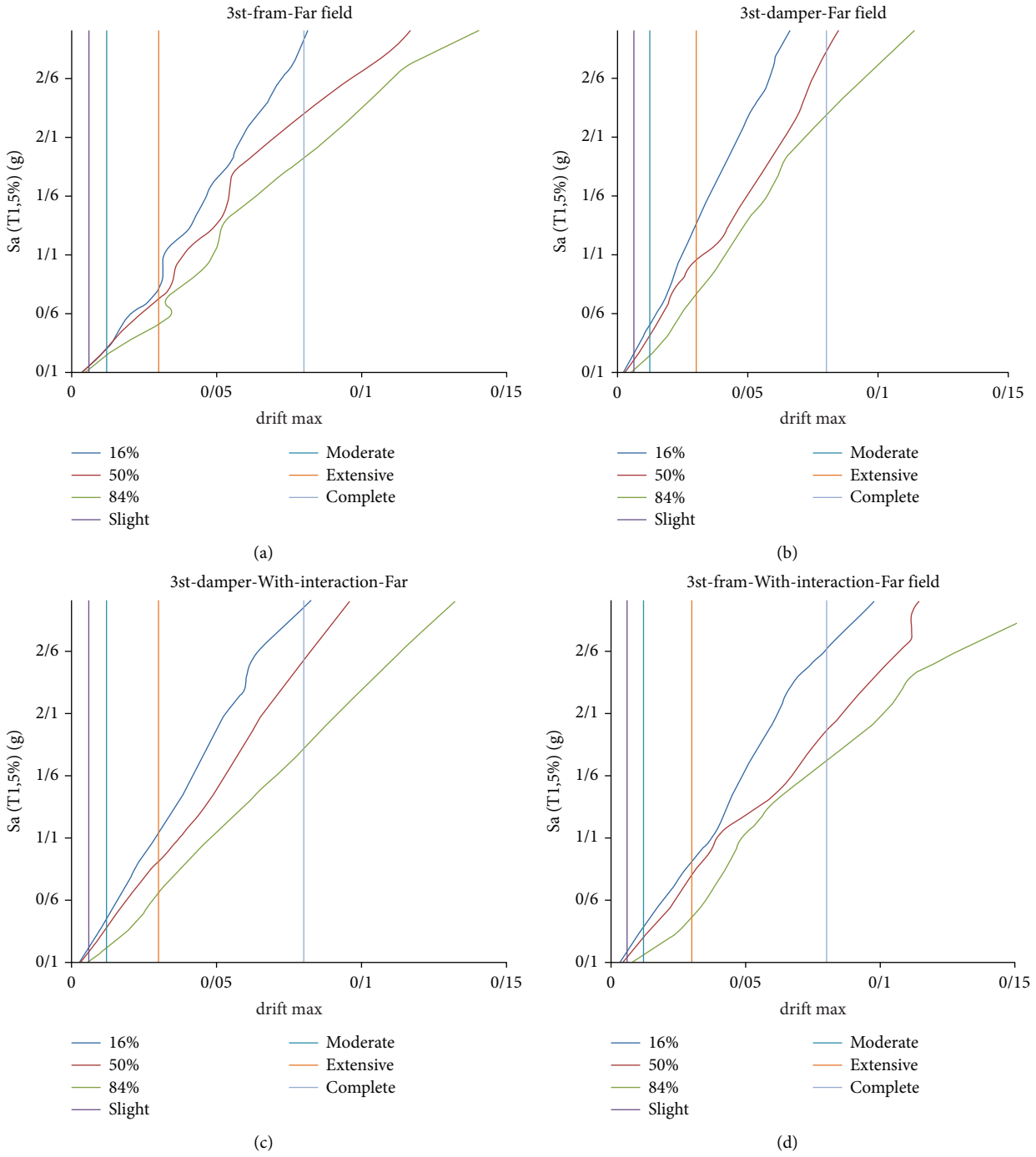

Figure 7: Summary of IDA curves for 16%, 50%, and 84% percentiles in 3-story ordinary moment resisting frame affected by far-field earthquakes. Examined cases: (a) with damper without considering SSI; (b) without Damper and SSI effect; (c) with damper and considering SSI; (d) without damper but considering SSI effect.

collapse region at a higher acceleration, which indicates better performance than other cases. Considering that the criterion of damage is interstory drift, the results show that the frame with damper reaches the level of failure at a higher spectral acceleration, respectively, compared to other frames. This indicates the damper's performance in reducing displacement between floors as one of the criteria for predicting damage and shows the effect of soil-structure interaction on increasing drift between floors and reaching the level of failure at lower spectral acceleration. The fragility curves of 3-story frames under seven pairs of far-field earthquakes are shown in Figure 8.

The fragility curve shows that the probability of structural failure in low failure mode occurs in less Sa values, and moderate, extensive, and complete failure modes occur in higher Sa values. In all curves, for low and moderate failure situations, the slope of the curve is first increased and then decreased. For extensive failure mode, the curves change

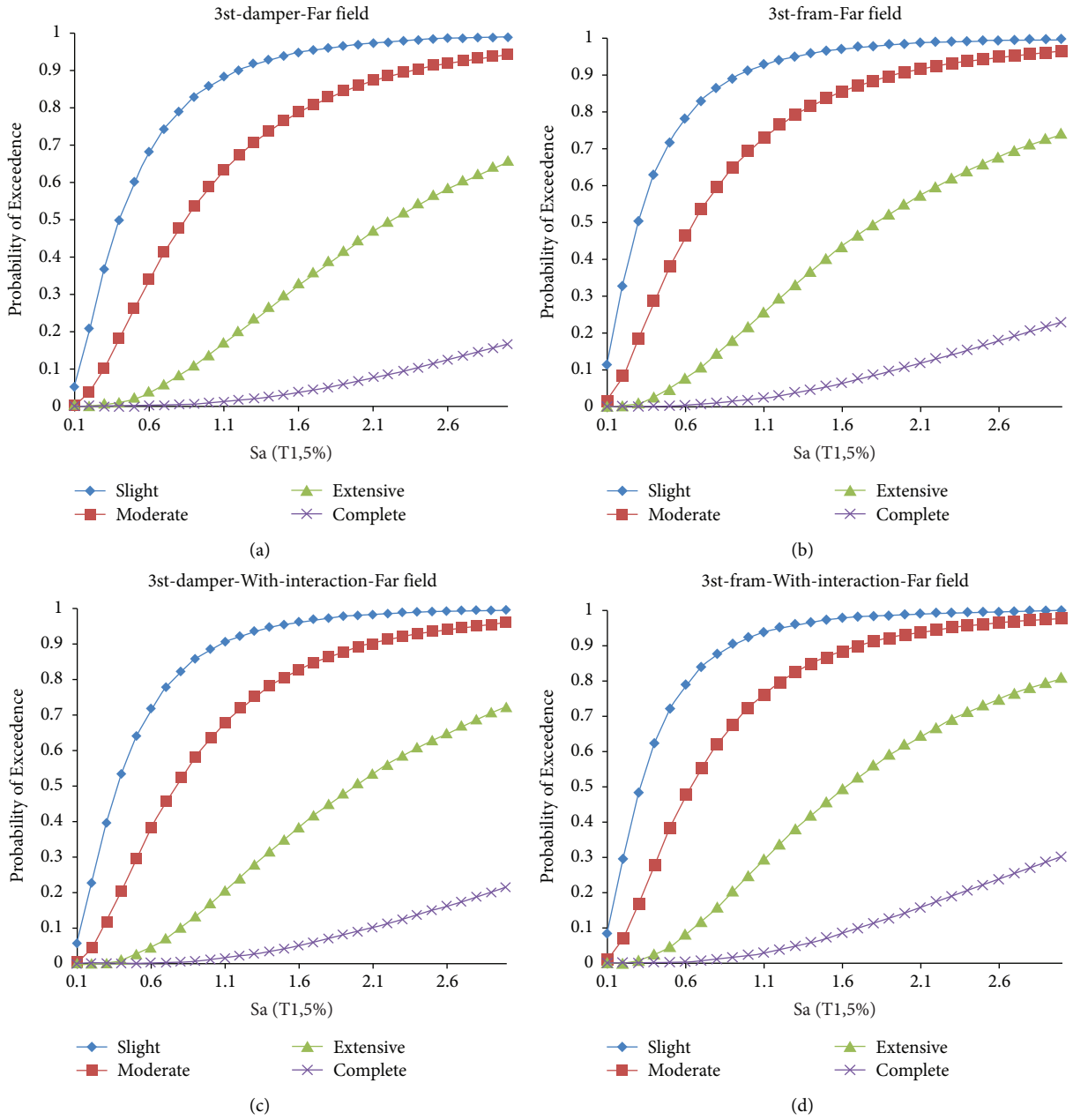

Figure 8: Fragility curves in 3-story ordinary moment resisting frame affected by far-field earthquakes. Examined cases: (a) with damper without considering SSI; (b) without Damper and SSI effect; (c) with damper and considering SSI; (d) without damper but considering SSI effect.

with an almost uniform slope. For complete failure mode, the slope changes are extremely small. According to the coefficient of acceleration scale of far-field earthquakes for 3-story structures, fragility occurs at a spectral acceleration of 1.63 g for type three soil. The results also show that soil-structure interaction has a significant effect on increasing the probability of structural failure. Also, dampers in both cases with and without soil-structure interaction reduce failure likelihood.

4.2. Eight Story Frame. The summary of the IDA curve with 16%, 50%, and 84% percentiles and fragility curves in an 8-story frame under seven pairs of near-field and far-field earthquakes is presented in Figure 9.

In an 8-story OMRF structure, like the previous models, the slope of the linear region in case (a), with damper and without SSI, is less than that in other states, which shows a softer behavior. In the cases with the damper, it enters the collapse region at a higher acceleration, which indicates better performance than other cases. Considering that the criterion of damage is interstory drift, the results show that the frame with a damper reaches the level of failure at a higher spectral acceleration than other frames. This indicates the damper's performance in reducing displacement

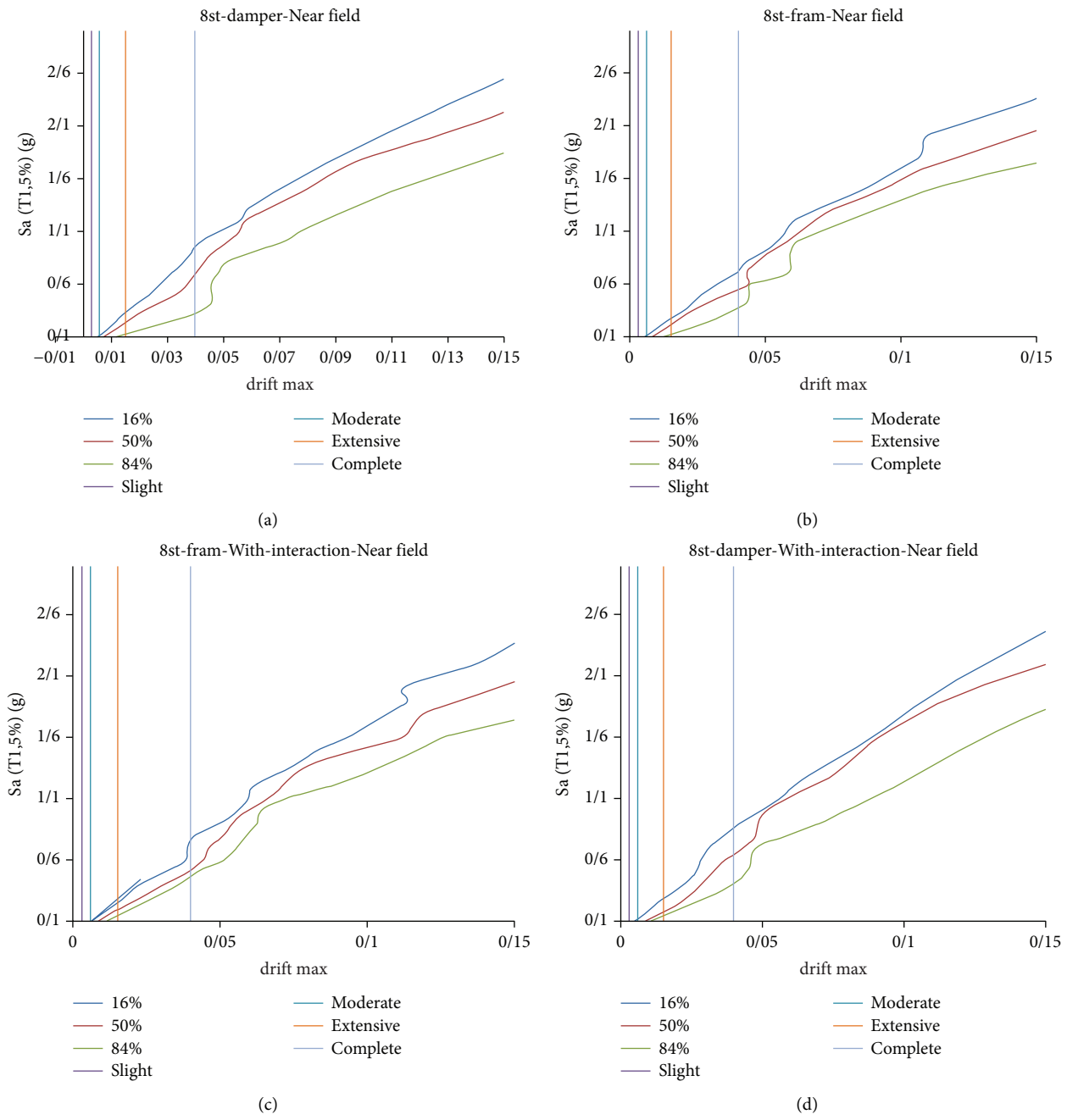

Figure 9: Summary of IDA curves for 16%, 50%, and 84% percentiles in 8-story ordinary moment resisting frame affected by near-field earthquakes. Examined cases: (a) with damper without considering SSI; (b) without damper and SSI effect; (c) with damper and considering SSI; (d) without damper but considering SSI effect.

between floors as one of the criteria for predicting damage and shows the effect of soil-structure interaction on increasing drift between floors and reaching the level of failure at lower spectral acceleration. The fragility curves of 8-story frames under seven pairs of near-field earthquakes are shown in Figure 10.

The fragility curve shows that the probability of structural failure in low failure mode occurs in less Sa values, and moderate, extensive, and complete failure modes occur in higher Sa values. In all curves, for low and moderate failure situations, the slope of the curve is first increased and then decreased. For extensive failure mode, the curves change with an almost uniform slope. For complete failure mode, the slope changes are extremely small. According to the coefficient of acceleration scale of far-field earthquakes for 3-story structures, fragility occurs at a spectral acceleration of 1.276 g for type three soil. The results also show that soil-structure interaction has a significant effect on increasing the

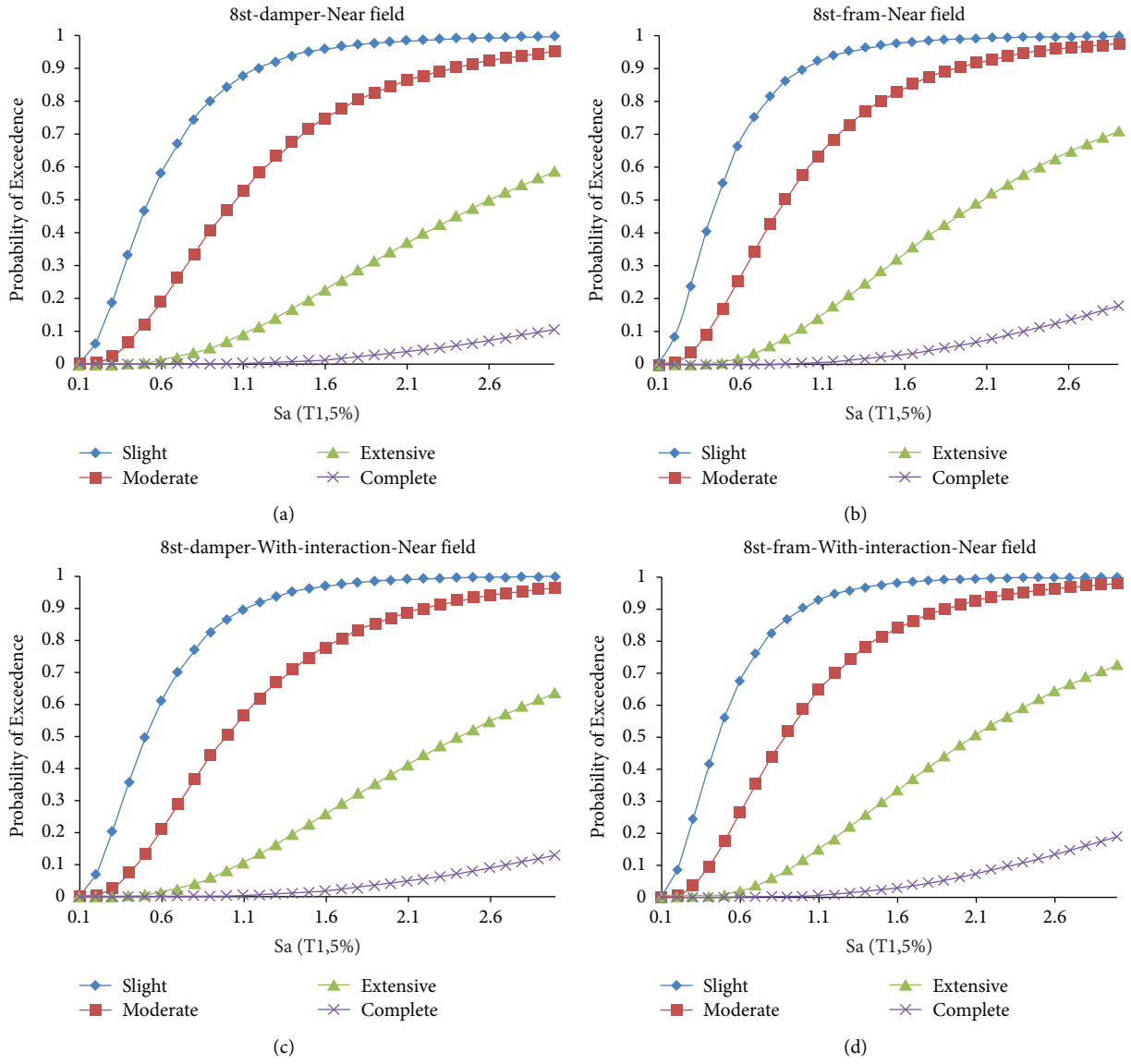

Figure 10: Fragility curves in 8-story ordinary moment resisting frame affected by near-field earthquakes. Examined cases: (a) with damper without considering SSI; (b) without damper and SSI effect; (c) with damper and considering SSI; (d) without damper but considering SSI effect.

probability of structural failure. Also, dampers in both cases with and without soil-structure interaction reduce failure probability. A summary of the IDA curve of a 3-story frame under seven pairs of far-field earthquakes is shown in Figure 11.

In the 8-story OMRF structure affected by far-field earthquakes, like the previous models, the slope of the linear region in the case (a), with damper and without SSI, is less than that in other states, which shows a softer behavior. In the cases with the damper, it enters the collapse region at a higher acceleration, which indicates better performance than other cases. Considering that the criterion of damage is interstory drift, the results show that the frame with damper reaches the level of failure at a higher spectral acceleration, respectively, compared to other frames. This indicates the damper's performance in reducing displacement between floors as one of the criteria for predicting damage and shows the effect of soil-structure interaction on increasing drift between floors and reaching the level of failure at lower spectral acceleration. The fragility curves of 8-story frames under seven pairs of far-field earthquakes are shown in Figure 12.

The figures mentioned above indicate that the probability of structural failure in low failure mode occurs in less Sa values, and moderate, extensive, and complete failure modes occur in higher Sa values. In all curves, for low and moderate failure situations, the slope of the curve is first increased and then decreased. For extensive failure mode, the curves change with an almost uniform slope. For complete failure mode, the slope changes are extremely small. According to the coefficient of acceleration scale of far-field earthquakes for 3-story structures, fragility occurs at a spectral acceleration of 2.12 g for type three soil. The results also show that soil-structure

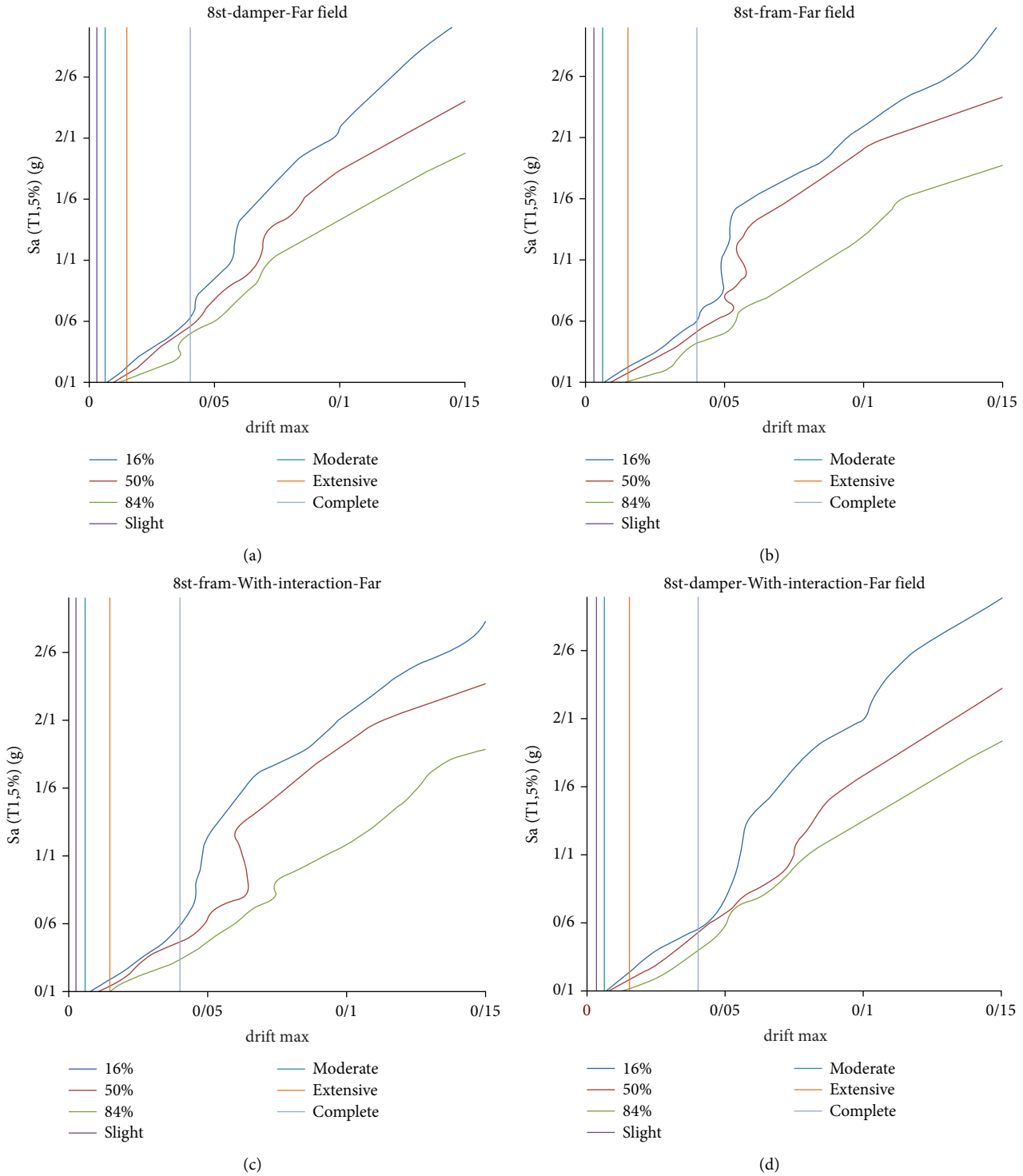

Figure 11: Summary of IDA curves for 16%, 50%, and 84% percentiles in 8-story ordinary moment resisting frame affected by far-field earthquakes. Examined cases: (a) with damper without considering SSI; (b) without damper and SSI effect; (c) with damper and considering SSI; (d) without damper but considering SSI effect.

interaction has a significant effect on increasing the probability of structural failure. Also, dampers in both cases with and without soil-structure interaction reduce the likelihood of failure.

4.3. 12-Story Frame. The summary of the IDA curve with 16%, 50%, and 84% fractiles and fragility curves in a 12-story frame under seven pairs of near-field and far-field earthquakes is presented in Figure 13.

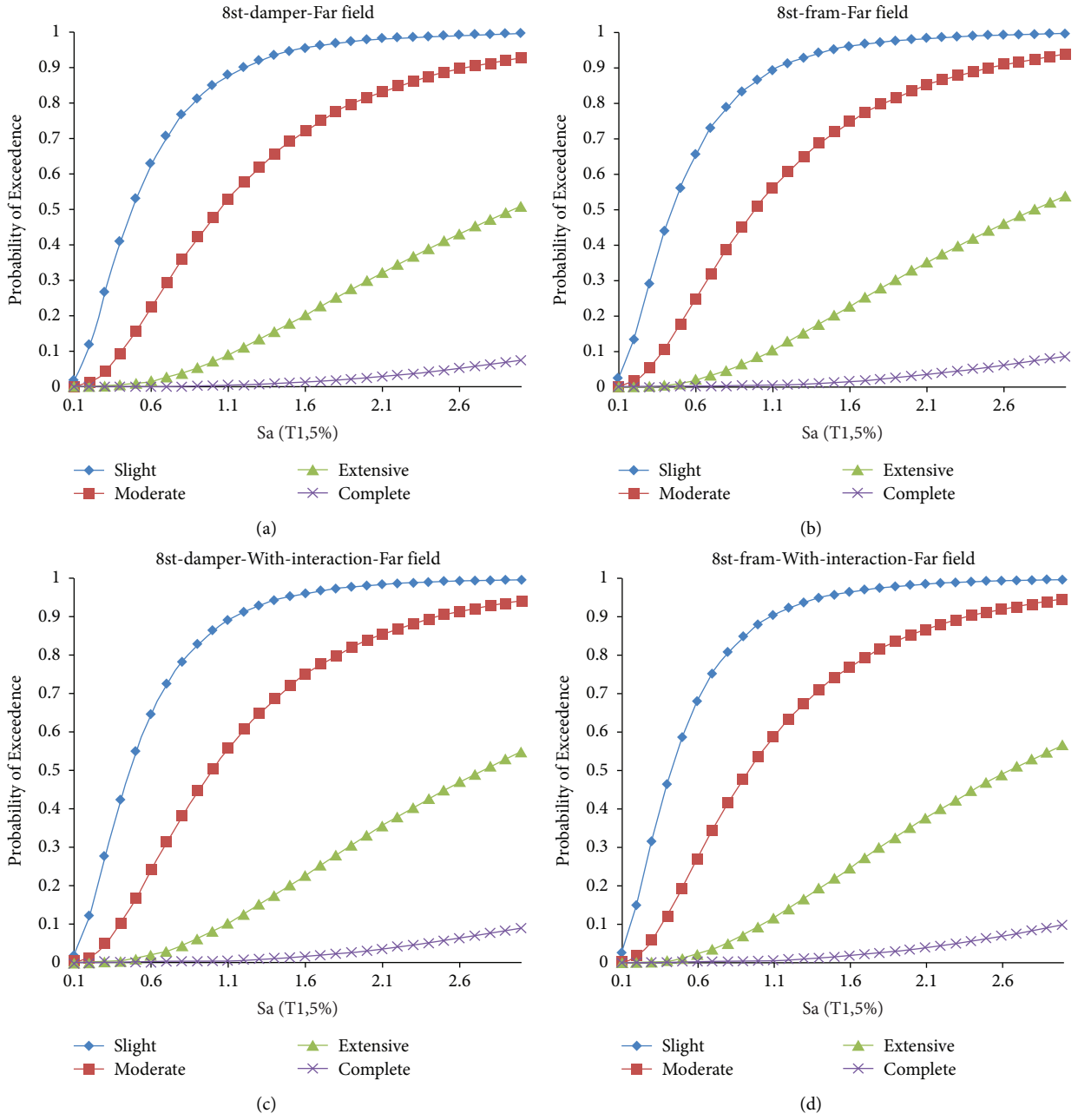

Figure 12: Fragility curves in 8-story ordinary moment resisting frame affected by far-field earthquakes. Examined cases: (a) with damper without considering SSI; (b) without damper and SSI effect; (c) with damper and considering SSI; (d) without damper but considering SSI effect.

In the 12-story OMRF structure affected by near-field earthquakes, like the other models, the slope of the linear region in the case (a), with damper and without SSI, is less than that in other states, which shows a softer behavior. In the cases with the damper, it enters the collapse region at a higher acceleration, which indicates better performance than other cases. Considering that the criterion of damage is interstory drift, the results show that the frame with a

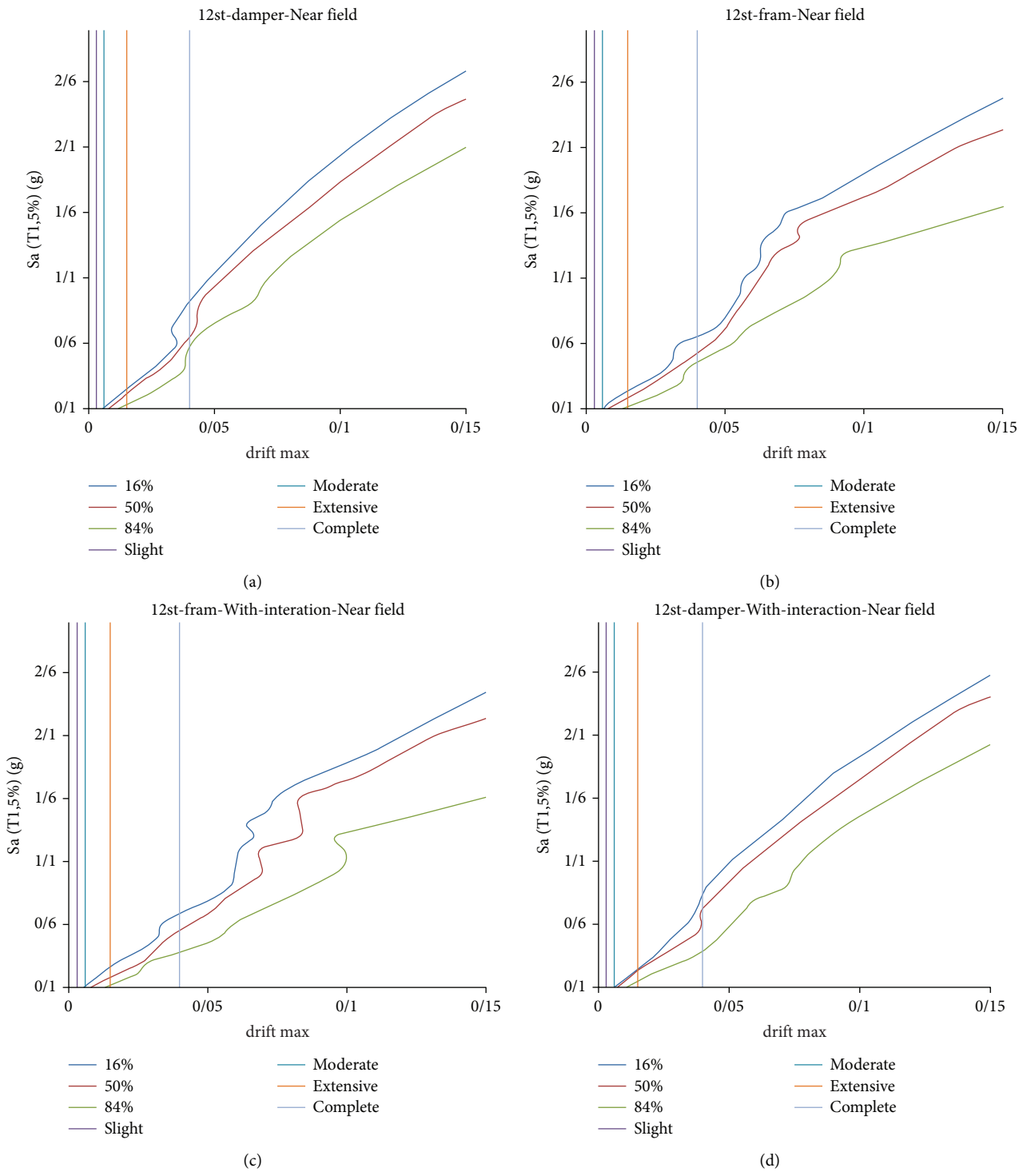

FIGURE 13: Summary of IDA curves for 16%, 50%, and 84% percentiles in 12-story ordinary moment resisting frame affected by near-field earthquakes. Examined cases: (a) with damper without considering SSI; (b) without damper and SSI effect; (c) with damper and considering SSI; (d) without damper but considering SSI effect.

damper reaches the level of failure at a higher spectral acceleration than other frames. This indicates the damper's performance in reducing displacement between floors as one of the criteria for predicting damage and shows the effect of soil-structure interaction on increasing drift between floors and reaching the level of failure at lower spectral acceler-

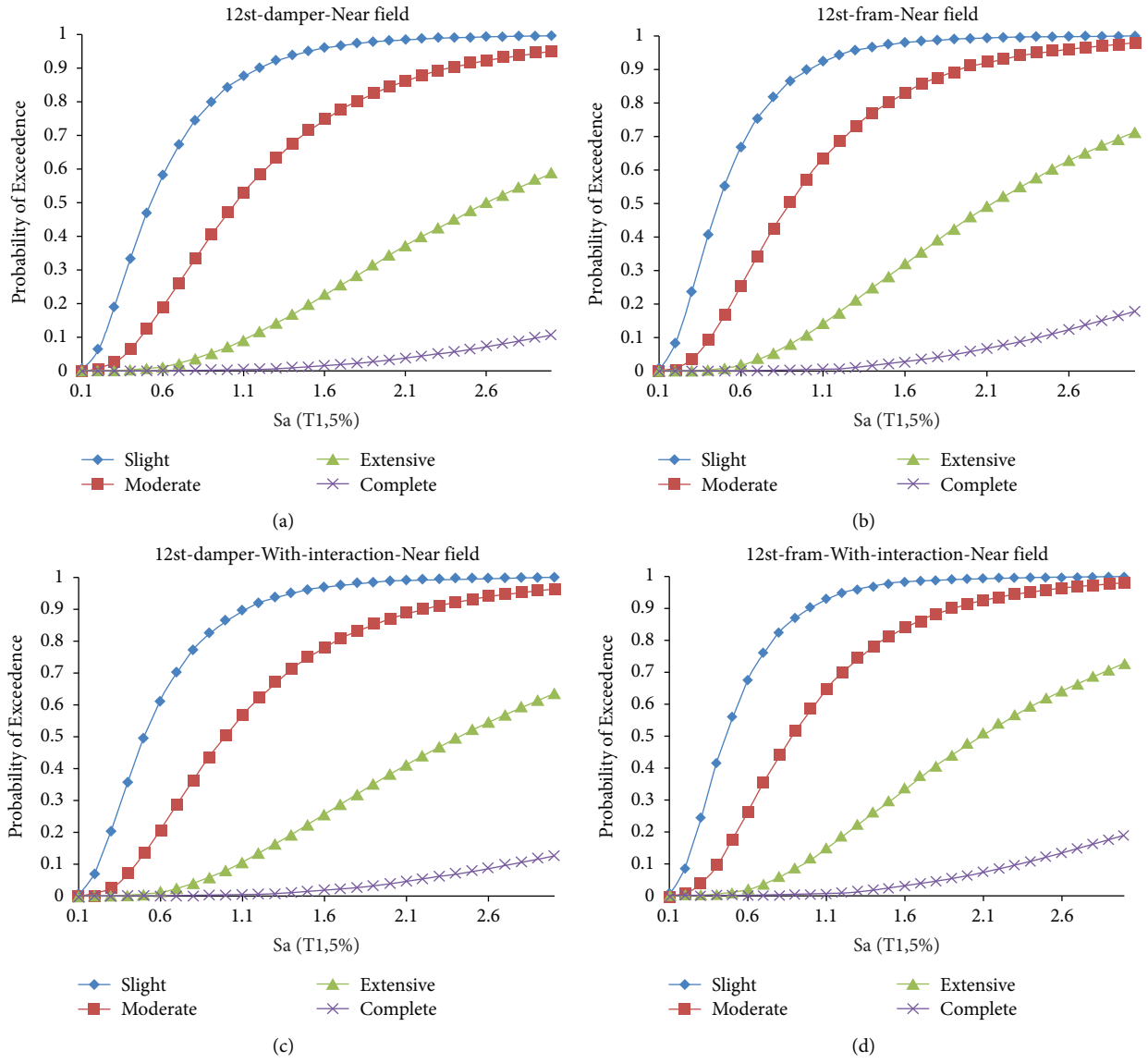

Figure 14: Fragility curves in 12-story ordinary moment resisting frame affected by near-field earthquakes. Examined cases: (a) with damper without considering SSI; (b) without damper and SSI effect; (c) with damper and considering SSI; (d) without damper but considering SSI effect.

ation. The fragility curves of 12-story frames under seven pairs of near-field acceleration are shown in Figure 14.

The fragility curve shows that the probability of structural failure in low failure mode occurs in less Sa values, and moderate, extensive, and complete failure modes occur in higher Sa values. In all curves, for low and moderate failure situations, the slope of the curve is first high and then decreased. For extensive failure mode, the curves change with an almost uniform slope. For complete failure mode, the slope changes are extremely small. According to the coefficient of acceleration scale of far-field earthquakes for 3-story structures, fragility occurs at a spectral acceleration of 1.344 g for type three soil. The results also show that soil-structure interaction has a significant effect on increasing the

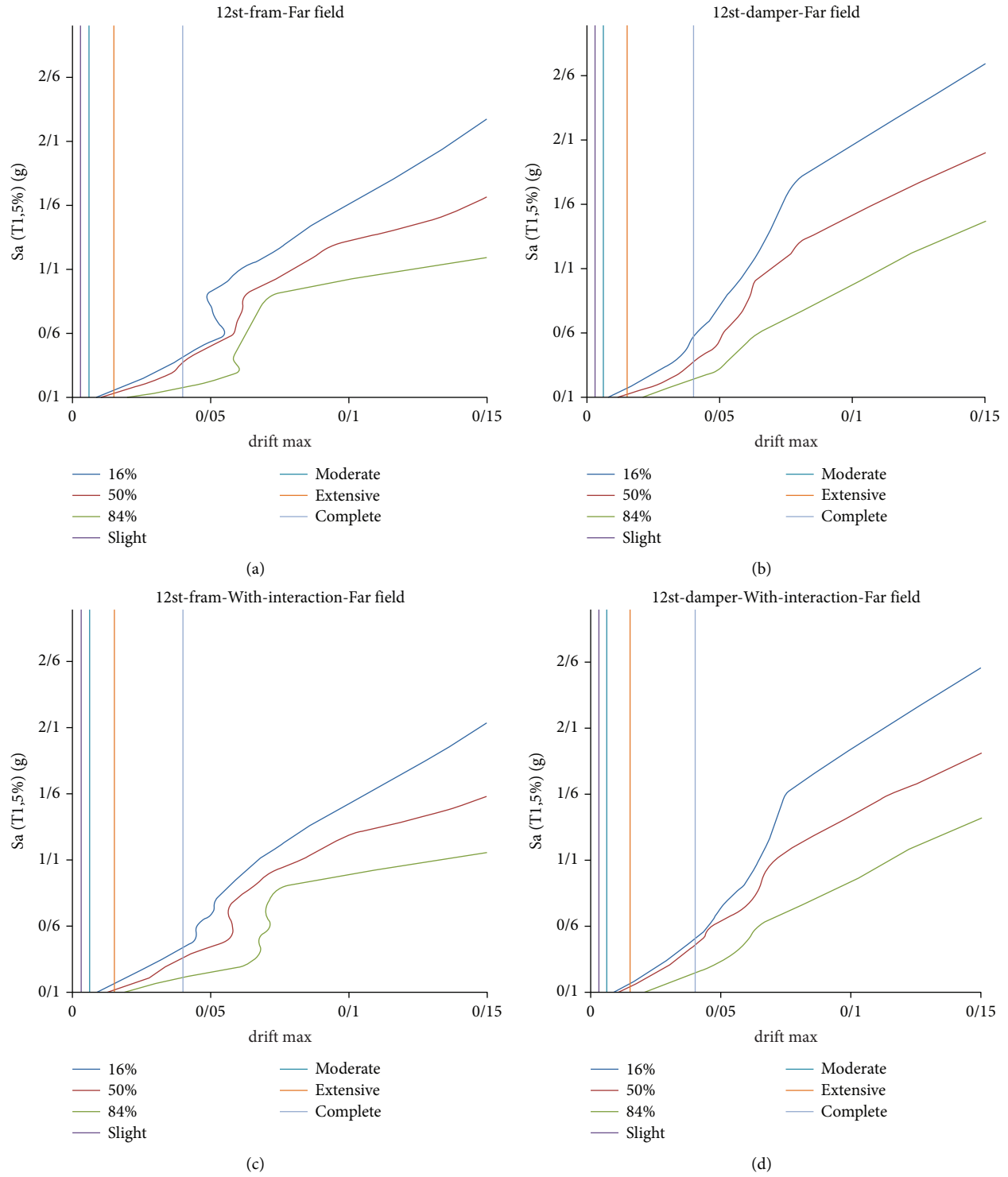

Figure 15: Summary of IDA curves for 16%, 50%, and 84% percentiles in 12-story ordinary moment resisting frame affected by far-field earthquakes. Examined cases: (a) with damper without considering SSI; (b) without damper and SSI effect; (c) with damper and considering SSI; (d) without damper but considering SSI effect.

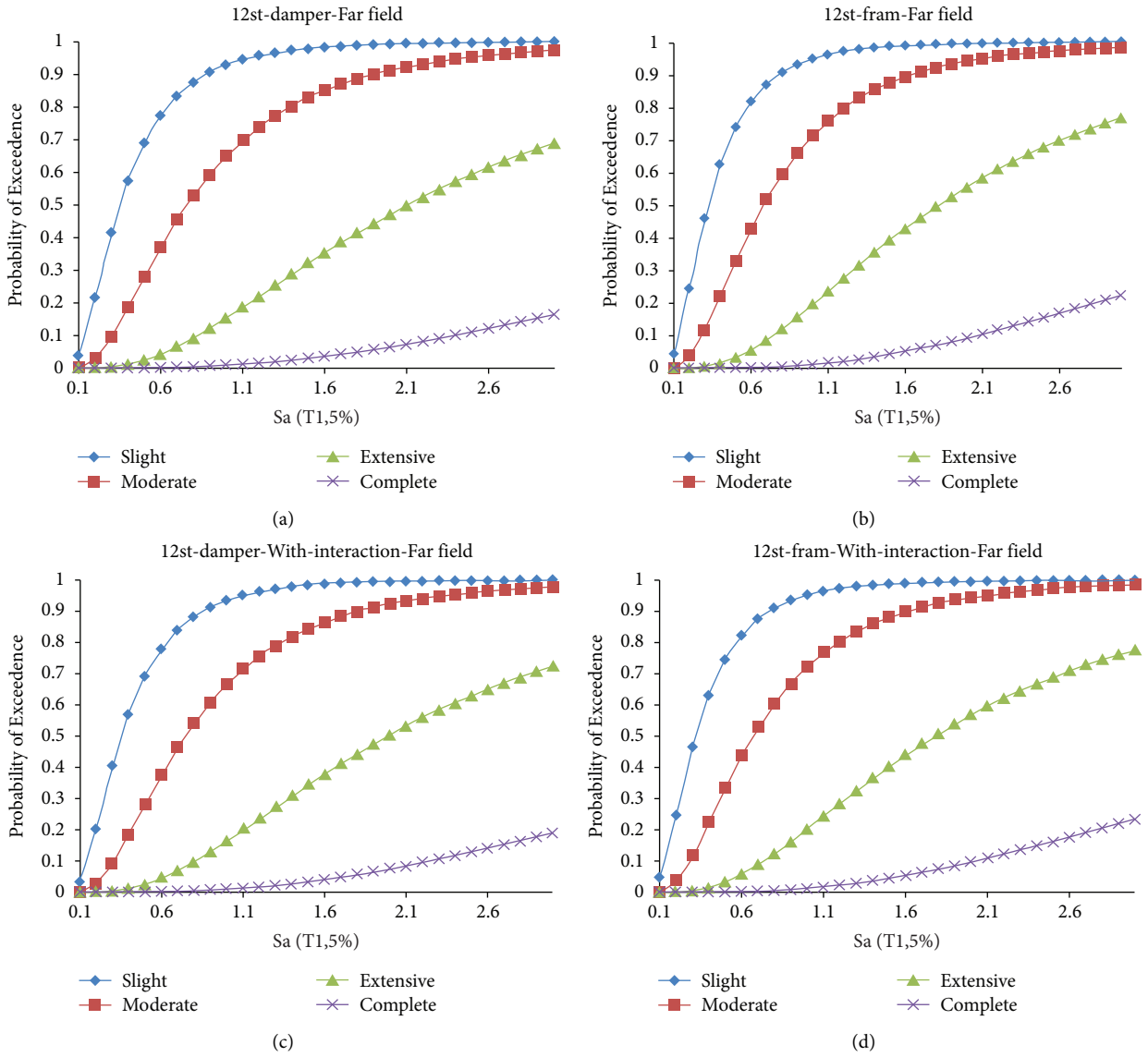

FIGURE 16: Fragility curves in 12-story ordinary moment resisting frame affected by far-field earthquakes. Examined cases: (a) with damper without considering SSI; (b) without damper and SSI effect; (c) with damper and considering SSI; (d) without damper but considering SSI effect.

probability of structural failure. Also, dampers in both cases with and without soil-structure interaction reduce failure likelihood. In the following, a summary of the IDA curve of a 3-story frame under seven pairs of far-field earthquakes is shown in Figure 15.

In the 8-story OMRF structure affected by far-field earthquakes, like the previous models, the slope of the linear region in the case (a), with damper and without SSI, is less than that in other states, which shows a softer behavior. In the cases with the damper, it enters the collapse region at a higher acceleration, which indicates better performance than other cases. Considering that the criterion of damage is interstory drift, the results show that the frame with a damper reaches the level of failure at a higher spectral acceleration than other frames. This indicates the damper's performance in reducing displacement between floors as one of the criteria for predicting damage and shows the effect of soil-structure interaction on increasing drift between floors and reaching the level of failure at lower spectral acceleration. The fragility curves of 12-story frames under seven pairs of far-field earthquakes are shown in Figure 16.

The fragility curve shows that the probability of structural failure in low failure mode occurs in less Sa values, and moderate, extensive, and complete failure modes occur in higher Sa values. In all curves, for low and moderate failure situations, the slope of the curve is first high and then decreased. For extensive failure mode, the curves change with an almost uniform slope. For complete failure mode, the slope changes are extremely small. According to the coefficient of acceleration scale of far-field earthquakes for 3-story structures, fragility occurs at a spectral acceleration of 2.12 g for type three soil. The results also show that soil-

structure interaction has a significant effect on increasing the probability of structural failure. Also, dampers in both cases with and without soil-structure interaction reduce the probability of failure.

5. Conclusion

In this study, three two-dimensional models of 3-, 8-, and 12-story ordinary steel moment frames were studied to evaluate the fragility of steel frames equipped with viscous dampers and consider SSI under near and far-field earthquakes. Each model was analyzed in OpenSees software. To draw the IDE curve, Sa (T1, 5%) was considered a parameter of seismic intensity, and interstory drift as a measure of damage intensity was selected. Then, the HAZUS instruction was used to draw the fragility curve based on the interstory drift ratio in 4 modes of slight, moderate, extensive, and complete failure. Therefore, the seismic response of the abovementioned structures is summarized as follows:

(1) The frame equipped with dampers, compared to other models, reaches the level of failure at a higher spectral acceleration, which indicates the damping function in reducing interstory drift.

(2) The effect of soil-structure interaction on increasing the displacement of stories and reaching the level of failure at spectral acceleration was less evident in all models.

(3) As the number of floors increases, the level of failure occurs at lower spectral acceleration.

(4) The level of failure occurs in the lower spectral acceleration in far-field earthquakes than in near-field earthquakes.

(5) In all models, low failure probability occurs in less Sa values (T1, 5%), and moderate, extensive, and complete failure modes occur in higher Sa values (T1, 5%), respectively.

The results support that as the number of floors of the studied structures increases, the probability of failure also increases. By comparing the fragility curves of the studied models under near-field and far-field accelerometers, it is clear that the probability of failure under far-field accelerometers is less than near-field [42].

Data Availability

Data are available and can be provided over the emails querying directly to the author at the corresponding author (amir_yousefpour@cmps2.iust.ac.ir).

Conflicts of Interest

The authors declare that they have no conflicts of interest.

References

[1] G. A. MacRae, D. V. Morrow, and C. W. Roeder, "near-fault ground motion effects on simple structures," *Journal of Structural Engineering*, vol. 127, no. 9, pp. 996–1004, 2001.

[2] P. Tothong and C. A. Cornell, "Structural performance assessment under near-source pulse-like ground motions using advanced ground motion intensity measures," *Earthquake Engineering & Structural Dynamics*, vol. 37, no. 7, pp. 1013–1037, 2008.

[3] B. Alavi and H. Krawinkler, "Behavior of moment-resisting frame structures subjected to near-fault ground motions," *Earthquake Engineering & Structural Dynamics*, vol. 33, no. 6, pp. 687–706, 2004.

[4] J. F. Hall, T. H. Heaton, M. W. Halling, and D. J. Wald, "Near-Source ground motion and its effects on flexible buildings," *Earthquake Spectra Journal*, vol. 11, no. 4, pp. 569–605, 1995.

[5] C. Champion and A. Liel, "The effect of near-fault directivity on building seismic collapse risk," *Earthquake Engineering and Structural Dynamics Journal*, 2012.

[6] A. R. Özuygur and E. Noroozinejad, "Influence of pulse-like near-fault ground motions on the base-isolated buildings with LRB devices," *Practice Periodical on Structural Design and Construction Journal*, vol. 26, no. 4, 2021.

[7] T. T. Song and G. F. Dargush, "Passive energy dissipation and active control," in *Structural Engineering Handbook*CRC Press LLC, Boca Raton, FL, USA, 1999.

[8] S. M. Zahrai and O. Mohammadi, "Seismic Behavior Upgrade of Steel Moment Frames Using Viscous Dampers and Determination of Their Proper Damping Forces," *Journal of Structural and Earthquake Analysis*, vol. 13, pp. 1–14, 2016.

[9] B. Silwal, O. E. Ozbulut, and R. J. Michael, "Seismic collapse evaluation of steel moment resisting frames with superelastic viscous damper," *Journal of Constructional Steel Research*, vol. 126, pp. 26–36, 2016.

[10] Y. Luo, H. Zheng, H. Zhang, and Y. Liu, "Fatigue reliability evaluation of aging prestressed concrete bridge accounting for stochastic traffic loading and resistance degradation," *Advances in Structural Engineering*, vol. 24, no. 13, pp. 3021–3029, 2021.

[11] S. Zhang, R. Y. Pak, and J. Zhang, "Three-dimensional frequency-domain green's functions of a finite fluid-saturated soil layer underlain by rigid bedrock to interior loadings," *International Journal of Geomechanics*, vol. 22, no. 1, Article ID 04021267, 2022.

[12] H. Liu, Z. Shi, J. Li et al., "Detection of road cavities in urban cities by 3D ground-penetrating radar," *Geophysics*, vol. 86, no. 3, pp. WA25–WA33, 2021.

[13] R. Moradi-dastjerdi, H. Momeni-Khabisi, and R. Baghbani, "Mesh-free dynamic analyses of FGM sandwich plates resting on a pasternak elastic foundation," *Mechanics of Advanced Composite Structures*, vol. 4, no. 2, pp. 153–168, 2017.

[14] H. Ghaffarzadeh, E. A. Dehrod, and N. Talebian, "Semi-active fuzzy control for seismic response reduction of building frames using variable orifice dampers subjected to near-fault earthquakes," *Journal of Vibration and Control*, vol. 19, no. 13, pp. 1980–1998, 2016.

[15] M. L. A. Prasad and E. A. Mazumder, "Use of viscous damper as an energy dissipative device in steel structures," *Int. J. Mech. Prod. Eng.*vol. 4, pp. 59–66, 2016.

[16] Y. Wang, H. Cheng, Q. Hu et al., "Pore structure heterogeneity of Wufeng-Longmaxi shale, Sichuan Basin, China: evidence from gas physisorption and multifractal geometries," *Journal of Petroleum Science and Engineering*, vol. 208, Article ID 109313, 2022.

[17] S. Jiang, Y. Zuo, M. Yang, and R. Feng, "Reconstruction of the Cenozoic tectono-thermal history of the dongpu depression, bohai bay basin, China: constraints from apatite fission track and vitrinite reflectance data," *Journal of Petroleum Science and Engineering*, vol. 205, Article ID 108809, 2021.

[18] C. Zhang and A. Ali, "The advancement of seismic isolation and energy dissipation mechanisms based on friction," *Soil Dynamics and Earthquake Engineering*, vol. 146, Article ID 106746, 2021.

[19] V. S. Balkanlou, M. R. B. Karimi, B. B. Azar, and A. Behravesh, "Evaluating effects of viscous dampers on optimizing seismic behavior of structures," *Int. J. Curr. Eng. Technol., Vl.*vol. 3, pp. 1150–1157, 2013.

[20] S. Silvestri, G. Gasparini, and T. Trombetti, "A five-step procedure for the dimensioning of viscous dampers to be inserted in building structures," *Journal of Earthquake Engineering*, vol. 14, no. 3, pp. 417–447, 2010.

[21] R. Milanchian and M. Hosseini, "Study of vertical seismic isolation technique with nonlinear viscous dampers for lateral response reduction," *Journal of Building Engineering*, vol. 23, pp. 144–154, 2019.

[22] D. De Domenico, G. Ricciardi, and I. Takewaki, "Design strategies of viscous dampers for seismic protection of building structures: a review," *Soil Dynamics and Earthquake Engineering*, vol. 118, pp. 144–165, 2019.

[23] J. Xu, W. Lan, C. Ren, X. Zhou, S. Wang, and J. Yuan, "Modeling of coupled transfer of water, heat and solute in saline loess considering sodium sulfate crystallization," *Cold Regions Science and Technology*, vol. 189, Article ID 103335, 2021.

[24] B. Li, G. Xiao, R. Lu, R. Deng, and H. Bao, "On feasibility and limitations of detecting false data injection attacks on power grid state estimation using D-FACTS devices," *IEEE Transactions on Industrial Informatics*, vol. 16, no. 2, pp. 854–864, 2019.

[25] T. Wang, W. Liu, J. Zhao, X. Guo, and V. Terzija, "A rough set-based bio-inspired fault diagnosis method for electrical substations," *International Journal of Electrical Power & Energy Systems*, vol. 119, Article ID 105961, 2020.

[26] M. Ghalami, M. Sc. Thesis, *The Effect of Soil-Structure Interaction in Tall Building Equipped with Passive Dampers under Seismic Loads"*, Department of Civil Engineering (Structure), University of Mohaghegh Ardabili, 2020.

[27] A. Amiri, S. Mohaseb, and J. khazaie, "The Effect of Soil-Structure Interaction on Seismic Retrofitting of Steel Structures," in *Proceedings of the 5th national and 1st international conference of steel and structures*, Tehran, Iran, July 2015.

[28] D. Šago, V. Martić, D. Šmida, N. Mayer, V. Lovretić, and I. Filipčić, "Telepsychiatry in the time of the COVID-19 and earthquake in zagreb as odysseus between scylla and Charybdis," *Psychiatria Danubina*, vol. 32, no. 3-4, pp. 478–481, 2020.

[29] G. Xiang, Y. Zhang, X. Gao, H. Li, and X. Huang, "Oblique detonation waves induced by two symmetrical wedges in hydrogen-air mixtures," *Fuel*, vol. 295, Article ID 120615, 2021.

[30] M. Arbabi and H. Tahghighi, "Influence of nonlinear SSI on the seismic response of low-to-mid-rise steel moment resisting frame buildings," *Journal of Structural and Construction Engineering*, vol. 7, no. 3, pp. 35–52, 2019.

[31] M. H. Hazus, *Hazus-MH MR4 Technical Manual: Multi-hazard Loss Estimation Methodology"*, FEMA, Washington, D.C, 2003.

[32] American National Standards Institute/American Institute of Steel Construction, *Seismic provisions for structural steel buildings*, ANSI/AISC, Chicago, IL, 2010.

[33] American Society of Civil Engineering (Asce), *Structural engineering Institute (SEI). "Minimum design loads for buildings and other structures*, ASCE Standard, Chicago, IL, 2010.

[34] M. NourEldin, A. Naeem, and J. Kim, "Life-cycle cost evaluation of steel structures retrofitted with steel slit damper and shape memory alloy-based hybrid damper," *Advances in Structural Engineering*, vol. 22, no. 1, pp. 3–16, 2019.

[35] X. Lu and Q. Zhou, "Dynamic analysis method of a combined energy dissipation system and its experimental verification," *Earthquake Engineering & Structural Dynamics*, vol. 31, no. 6, pp. 1251–1265, 2002.

[36] C. Fang, Y. Ping, Y. Chen, M. Yam, J. Chen, and W. Wang, "Seismic performance of self-centering steel frames with SMA-viscoelastic hybrid braces," *Journal of Earthquake Engineering*, pp. 1–28, 2020.

[37] M. Khakpour and M. Hajialilue Bonab, "Soil-structure-interaction using Cone model in time domain for horizontal and vertical motions in layered half space," *Journal of Earthquake Engineering*, vol. 24, no. 4, pp. 529–554, 2018.

[38] D. Vamvatsikos and C. A. Cornell, "Incremental dynamic analysis," *Earthquake Engineering & Structural Dynamics*, vol. 31, no. 3, pp. 491–514, 2002.

[39] P. Christovasilis, G. P. Cimellaro, S. Barani, and S. Foti, "On the selection and scaling of ground motions for fragility analysis of structures," in *Proceedings of the 2nd European Conference of Earthquake Engineering and Seismology*, 2014.

[40] PEER Ground Motion Database, https://peer.berkeley.edu/peer-strong-ground-motion-databases, 2011.

[41] C. Fang, Q. Zhong, W. Wang, S. Hu, and C. Qiu, "Peak and residual responses of steel moment-resisting and braced frames under pulse-like near-fault earthquakes," *Engineering Structures*, vol. 177, pp. 579–597, 2018.

[42] OpenSees, *Open System for Earthquake Engineering Simulation", Pacific Earthquake Engineering Research Center*, University of California, Berkeley, California, 2007, http://opensees.berkeley.edu/.